SUPPORTING INFORMATION

Retaining the 3D Framework of Zinc Sponge Anodes upon Deep Discharge in Zn-Air Cells

Joseph F. Parker, Eric S. Nelson,[†] Matthew D. Wattendorf,[‡]*
*Christopher N. Chervin, Jeffrey W. Long, and Debra R. Rolison**

Surface Chemistry Branch, Code 6170, U. S. Naval Research Laboratory, Washington, DC 20375, USA

[†]Pathways Student

[‡]Student Volunteer

* Corresponding Authors:
(JFP) E-mail: joseph.parker@nrl.navy.mil. Phone: (202) 767–0219.
(DRR) E-mail: rolison@nrl.navy.mil. Phone: 767-3617.

DERIVATION OF ZnO THICKNESS

Assuming a d_{50} of 45-μm spherical Zn particles, the mass of an individual Zn particle is estimated to be:

$$m_{Zn}^{o} = V_{Zn}^{o}\rho_{Zn} = \frac{4}{3}\pi(r_{Zn}^{o})^{3}\rho_{Zn} \quad \text{(S1)}$$

The mass of Zn metal remaining as it undergoes discharge and the mass of forming ZnO is related to the depth-of-discharge (defined as a fraction) by the following equations:

$$m_{Zn} = f_{Zn}m_{Zn}^{o} = (1 - DOD)m_{Zn}^{o} \quad \text{(S2)}$$

$$m_{ZnO} = DOD \times m_{Zn}^{o} \times \frac{MW_{ZnO}}{MW_{Zn}} \quad \text{(S3)}$$

The volume occupied by the Zn core is given by the equation below:

$$V_{Zn} = \frac{4}{3}\pi r_{Zn}{}^{3} = \frac{m_{Zn}}{\rho_{Zn}} \quad \text{(S4)}$$

Combining Eq. S4, Eq. S2, and Eq. S1 yields:

$$r_{Zn} = ((r_{Zn}^{o})^{3} \times (1 - DOD))^{1/3} \quad \text{(S5)}$$

The volume occupied by the ZnO is given by the equation below:

$$V_{ZnO} = \frac{m_{ZnO}}{\rho_{ZnO}} \quad \text{(S6)}$$

Combining Eq. S6, Eq. S3, and Eq. S1 yields:

$$V_{ZnO} = DOD \times \frac{4}{3}\pi(r_{Zn}^{o})^{3} \times \frac{\rho_{Zn}}{\rho_{ZnO}} \times \frac{MW_{ZnO}}{MW_{Zn}} \quad \text{(S7)}$$

The generic equations for the volume of a shell on a sphere are as follows:

$$V_{shell} = \frac{4}{3}\pi(r_{tot}^{3} - r_{core}^{3}) \quad \text{(S8)}$$

$$\text{where} \quad r_{tot} = r_{core} + t \quad \text{(S9)}$$

Combining Eq. S8 and Eq. S9 and solving for t yields:

$$t = \sqrt[3]{\frac{3}{4\pi}V_{shell} + (r_{core})^{3}} - r_{core} \quad \text{(S10)}$$

Substituting V_{shell} for V_{ZnO} (Eq. S7) and r_{core} for r_{Zn} (Eq. S5) yields:

$$t_{ZnO} = \sqrt[3]{(r_{Zn}^{o})^{3}(1 - DOD) + DOD(r_{Zn}^{o})^{3}\frac{\rho_{Zn}}{\rho_{ZnO}}\frac{MW_{ZnO}}{MW_{Zn}}} - ((r_{Zn}^{o})^{3} \times (1 - DOD))^{1/3} \quad \text{(S11)}$$

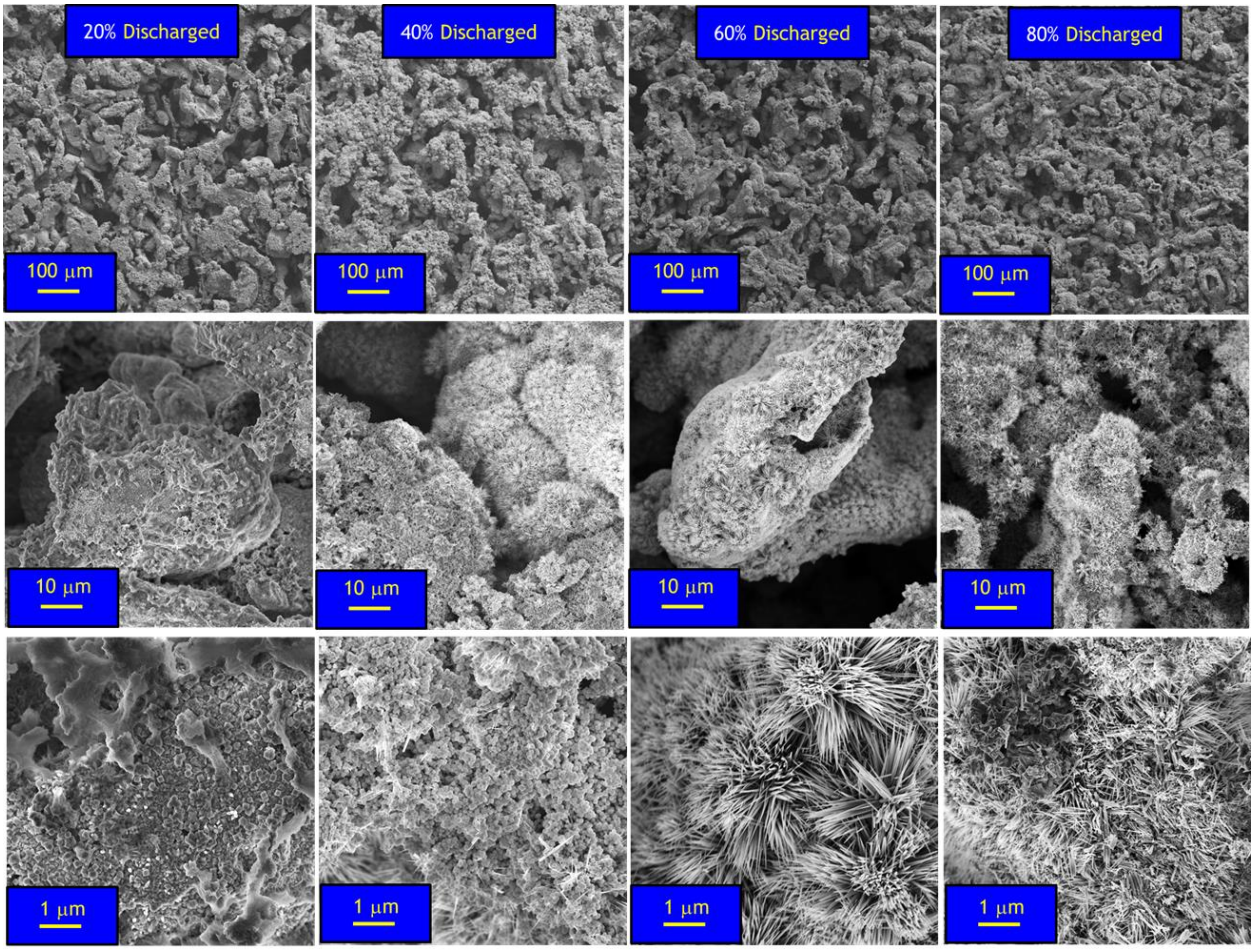

Figure S1. Replicate experiment of the micrographs in the main text. Scanning electron micrographs of the post–discharged microstructure at the separator-facing boundary of a discharged Zn sponge anode. This series of micrographs represents four different Zn sponges discharged to the labeled depths-of-discharge at 5 mA cm^{-2}. The monolithic porous 3D structure is retained at all levels of discharge. As discharge progresses, needle-like crystals of ZnO form, first in islands that eventually coalesce to a uniform carpet-like deposit throughout the electrode structure.

Table S1. Parameters for electrochemical discharge tests of Zn–air cells (replicate to data presented in main text).

Experiment	depth-of-discharge (%)	specific capacity (mA h g_{Zn}^{-1})	$R_{cell,\ initial}$ [b] ($\Omega\ cm^{-2}$)	$R_{cell,\ post\text{-}discharge}$ [b] ($\Omega\ cm^{-2}$)
3D Zn-20 [a] **(repeat)**	20	164	1.37	1.15
3D Zn-40 [a] **(repeat)**	40	328	4.50	3.08
3D Zn-60 [a] **(repeat)**	60	492	1.10	1.03
3D Zn-80 [a] **(repeat)**	80	656	1.37	1.20

[a] These data are derived from one set of 20–40–60–80% DOD discharged at 5 mA cm^{-2} (C/40 rate)
[b] R_{cell} ($\Omega\ cm^{-2}$) is calculated from the cell resistance divided by the geometric area of the full cell.

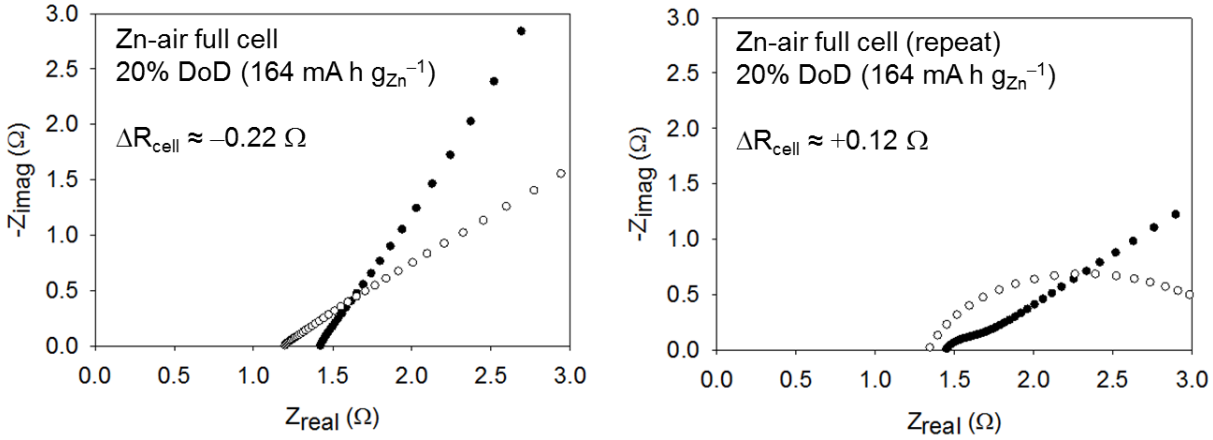

Figure S2. EIS measurements before (●) and after (○) from duplicate experiments of Zn–air cells discharged to 20% DoD. The series presented in Table 1 of the main text reveals that the cell resistance increases in the 40% and 60% case, but decreases in the 20, 80, and 91% cases, all with variations of only a few hundred milliohms (ΔR_{cell} avg. = –0.17 Ω ± 0.67 Ω). While the total cell resistance remains low, we attribute the inconsistency in the sign of the change to variations related to cell construction. The control experiment above demonstrates the very minor variations that can occur in seemingly identical experiments. However, none of the 3D Zn sponges change in the magnitude observed in the commercial Zn–air cells when subjected to similar tests (ΔR_{cell} increases ~6-fold).

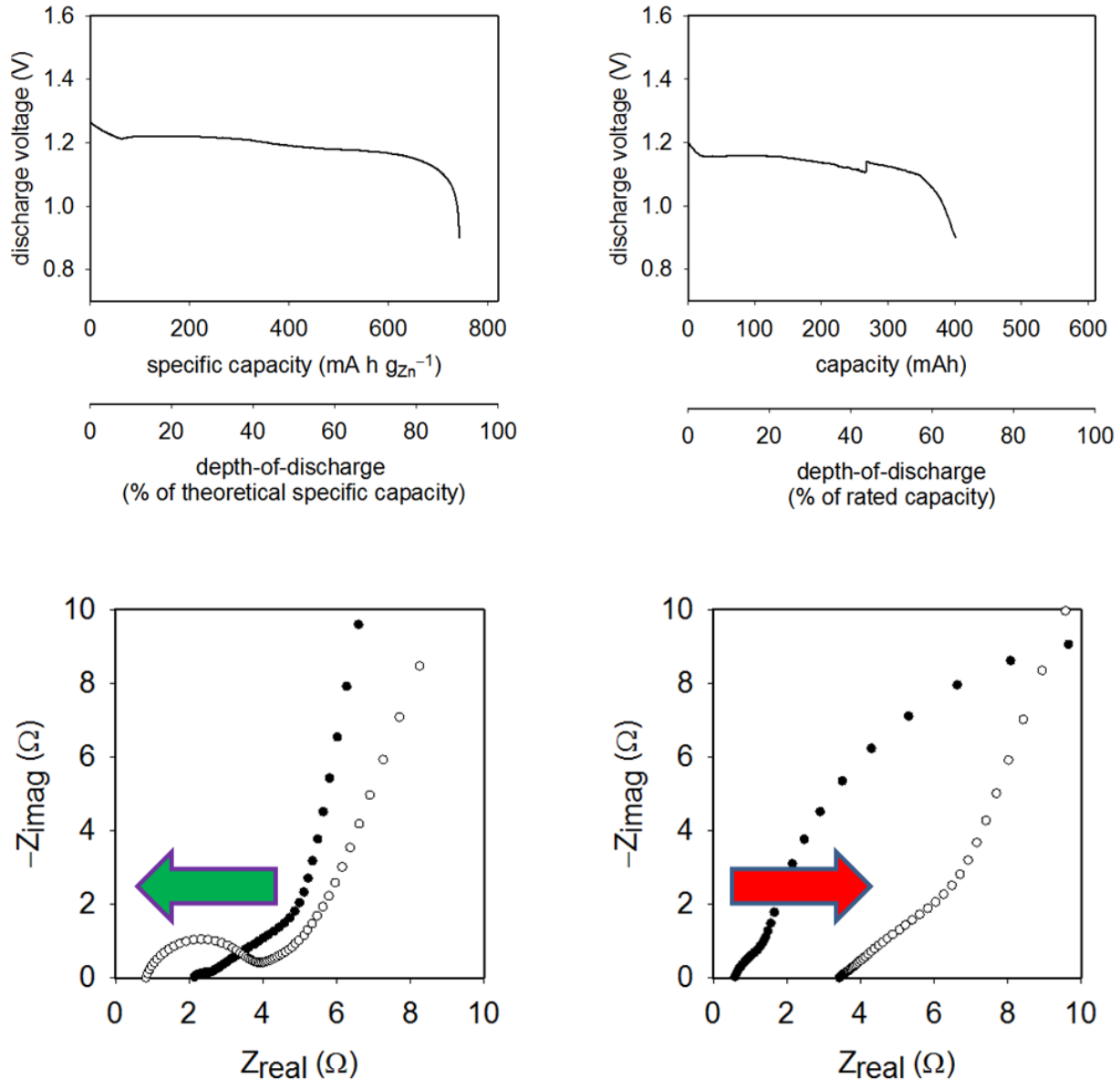

Figure S3. (**left**) Discharge of primary Zn–air cell at a C/15 rate (9.3 mA) to 91% depth-of-discharge using a 3D Zn sponge electrode versus an E4 air cathode (Electric Fuel, Inc.) with a single Celgard 3501 separator. The cell resistance *decreases* from 2.12 Ω (before, ●) to 0.83 Ω (after, ○), indicating retention of inner electronic wiring post–discharge. (**right**) Discharge of a commercial (Duracell 675) Zn–air battery at a C/40 rate (15.25 mA; the C/15 rate was too demanding for these commercial cells), achieving 401 mA h of its rated 610 mA h (69% depth-of-discharge). The cell resistance *increases* from 0.56 Ω (before, ●) to 3.43 Ω (after, ○), attributed to accumulation of (semi)conducting ZnO in the non-through-connected anode structure.

Table S2. Initial and final mass of Zn sponges discharged to a series of depths, compared with the expected mass increase associated with conversion of Zn to ZnO. The average post-discharged masses deviate from the expected value by an average of –1.7% ± 5.2%, indicating retention of the reaction products to the surfaces of the Zn sponge anodes.

Depth-of-discharge at Zn (%)	Initial mass Zn (g)	Predicted mass post-discharge (g)	Measured mass post-discharge (g)	Deviation (%)
20	0.2511	0.2634	0.2455	–7.3
40	0.2734	0.3002	0.2793	–7.5
60	0.2693	0.3088	0.3118	1.0
77	0.1546	0.1837	0.1899	3.3
80	0.2379	0.2845	0.2892	1.6
91	0.1703	0.2082	0.2060	–1.1
			Average Deviation	–1.7% ± 5.2%

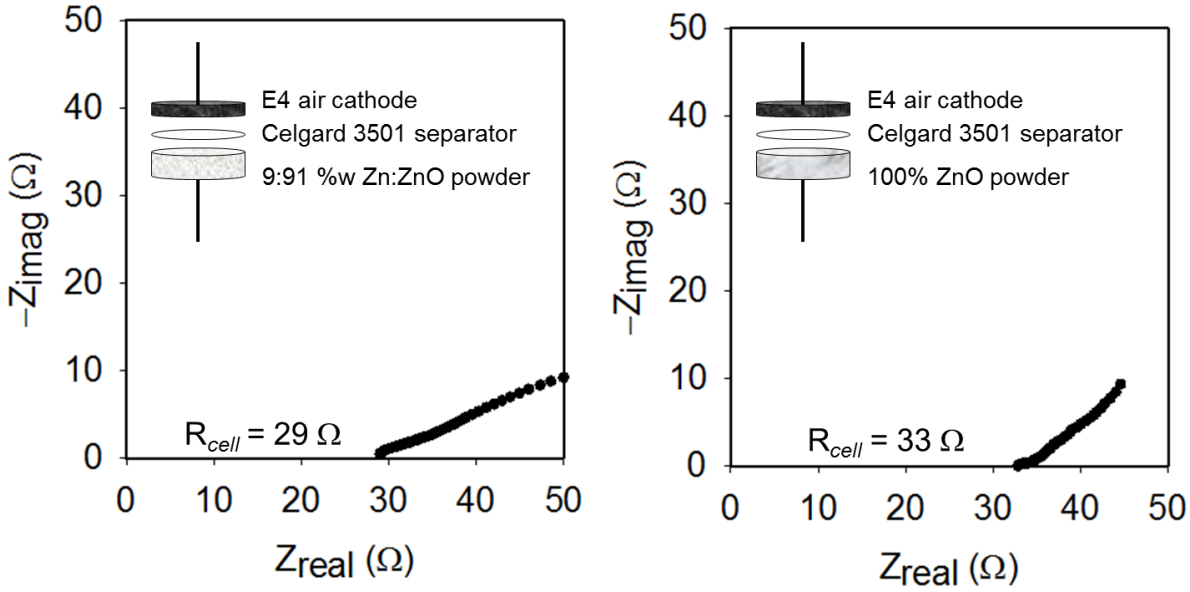

Figure S4. (**left**) Control experiment using E4 air cathode and pressed (at 7000 psi) anode comprising 9 wt% Zn and 91 wt% ZnO, simulating the final composition of the 91% discharged Zn–air from Figure S3, but inducing a state in which the anode is *not* wired in 3D. The percentage of Zn^0 present in the pressed anode is not sufficient to support a percolation path to rival the low resistance observed in the 91% discharged 3D Zn–air cell (0.83 Ω), yet it does reduce the resistance relative to (**right**) a Zn–air cell comprising only ZnO as the negative electrode.

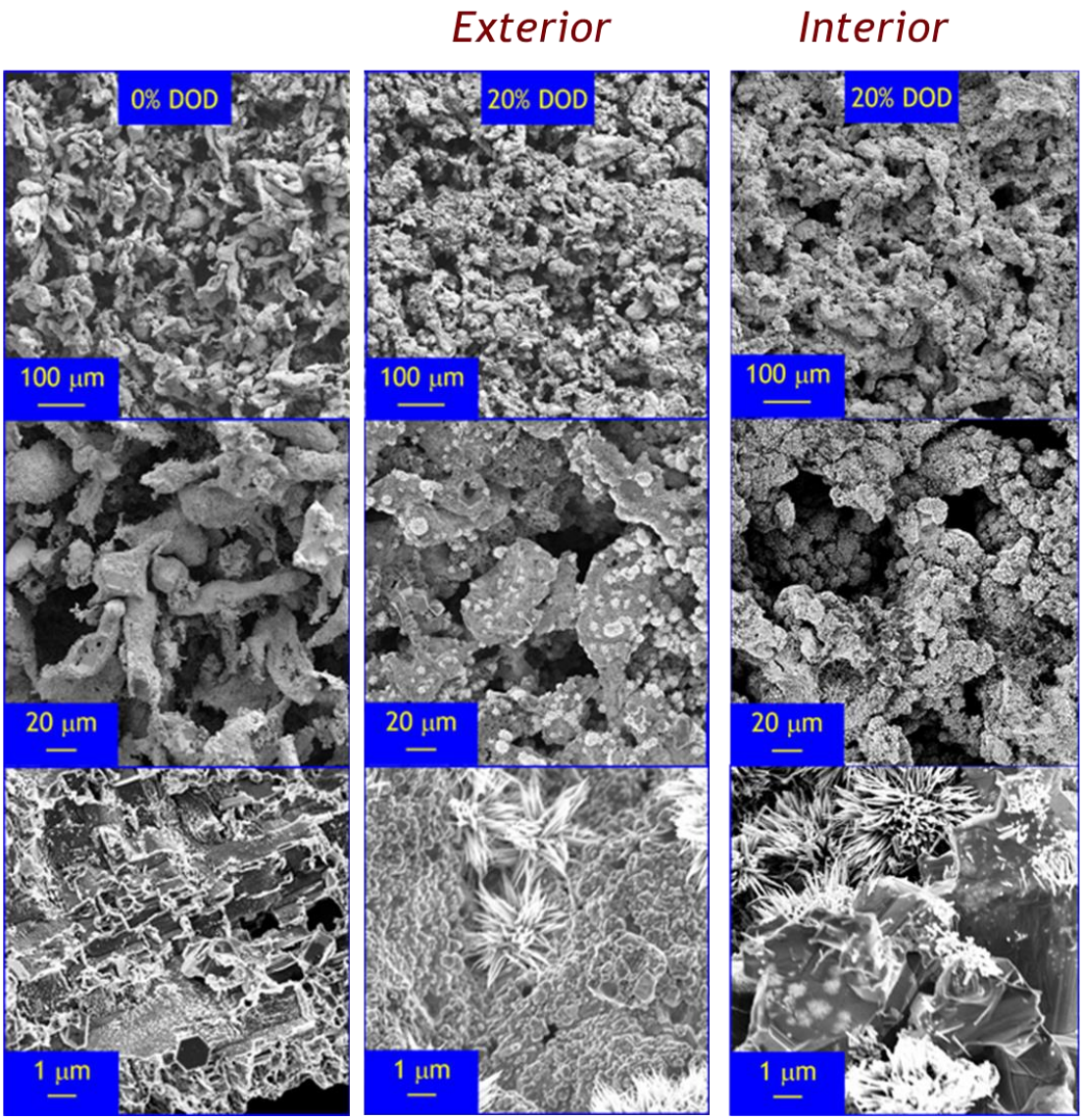

Figure S5. Scanning electron micrographs of the Zn sponge microstructure in its (**left**) pre–discharged state and after discharging to 20% DOD, revealing the progression of ZnO formation in the (**middle**) exterior/separator-facing boundary and (**right**) interior of the Zn sponge anode. (Alternate view of Figures 2 & 3)

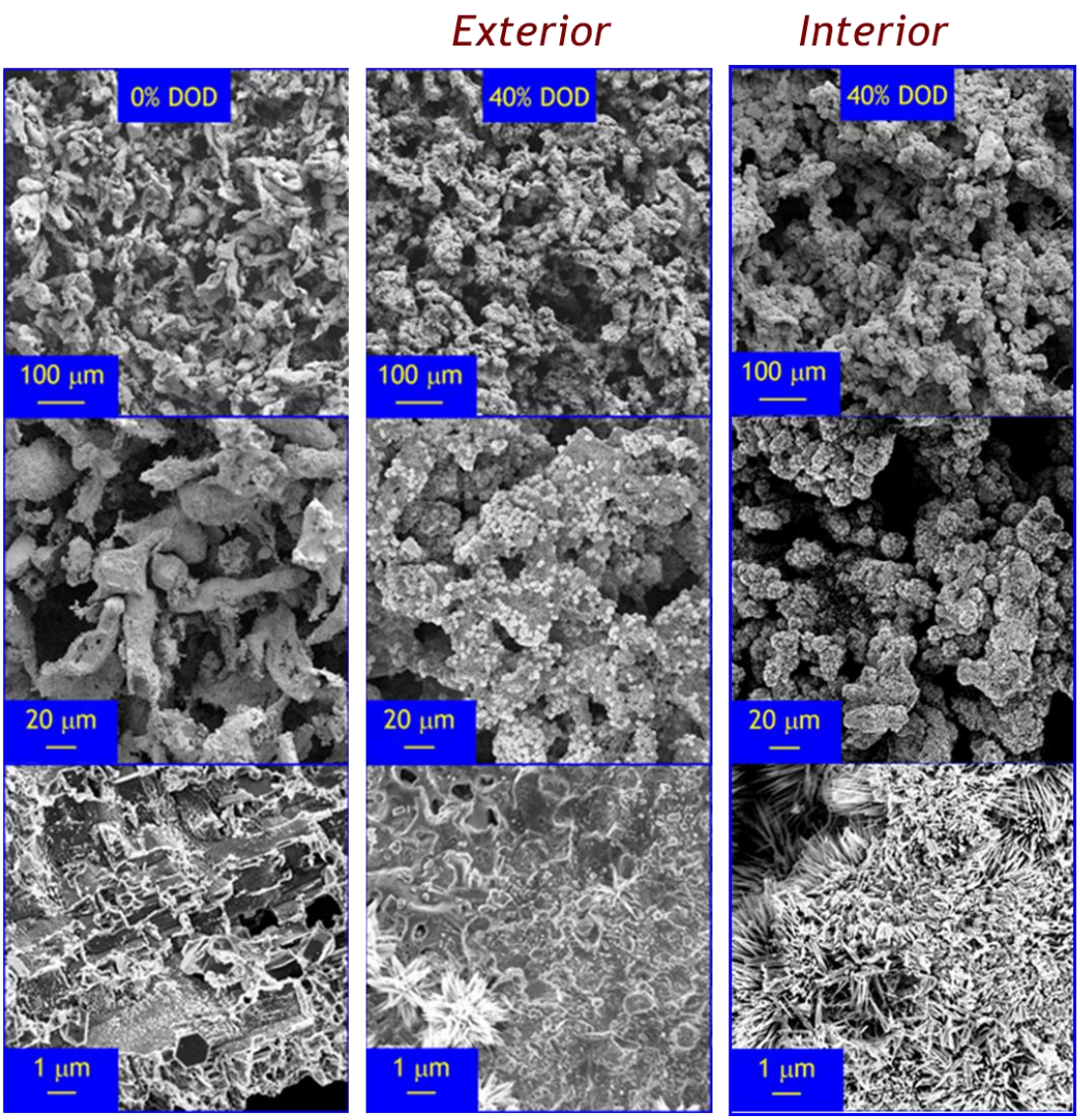

Figure S6. Scanning electron micrographs of the Zn sponge microstructure in its (**left**) pre–discharged state and after discharging to 40% DOD, revealing the progression of ZnO formation in the (**middle**) exterior/separator-facing boundary and (**right**) interior of the Zn sponge anode. (Alternate view of Figures 2 & 3)

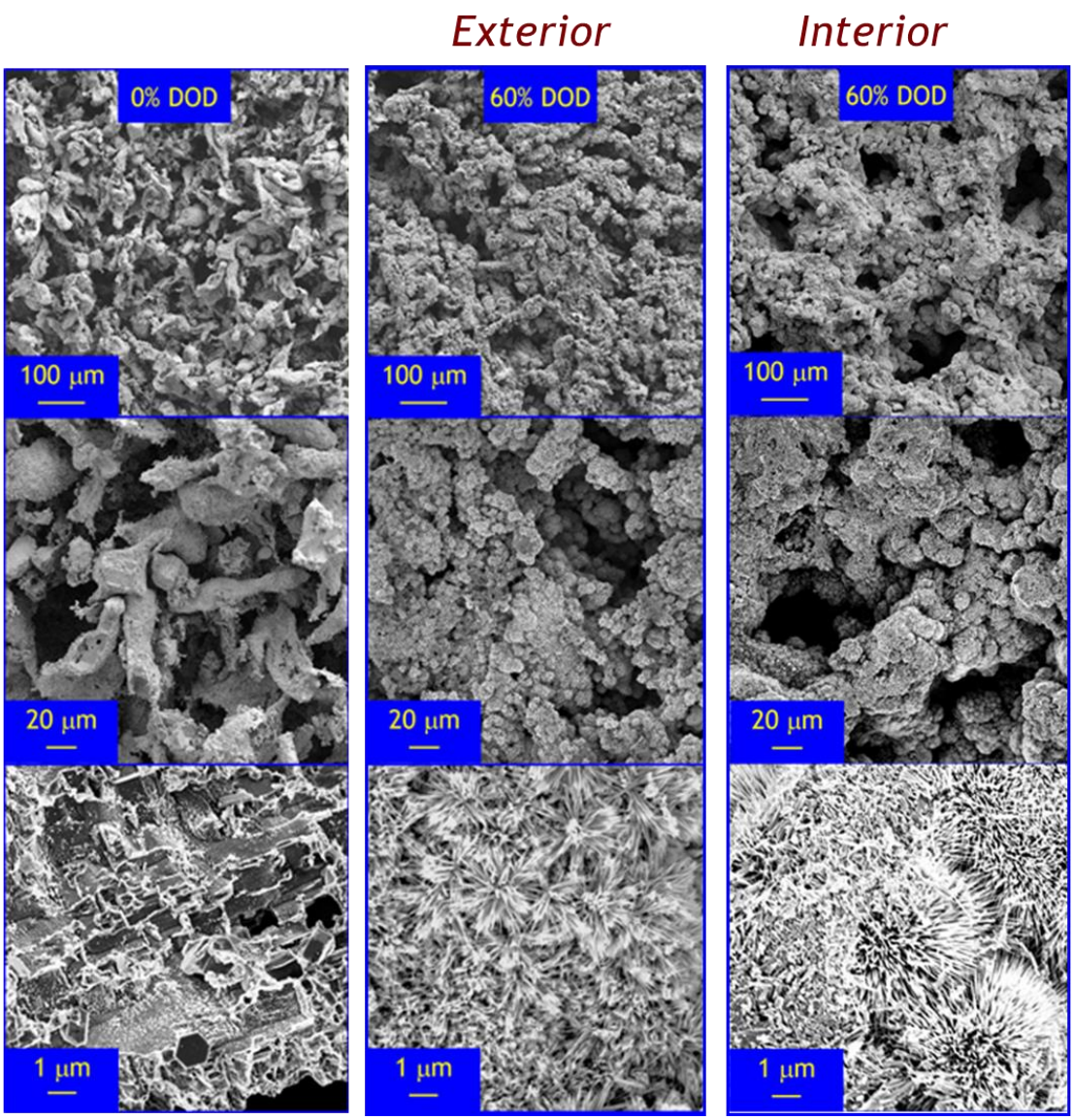

Figure S7. Scanning electron micrographs of the Zn sponge microstructure in its (**left**) pre–discharged state and after discharging to 60% DOD, revealing the progression of ZnO formation in the (**middle**) exterior/separator-facing boundary and (**right**) interior of the Zn sponge anode. (Alternate view of Figures 2 & 3)

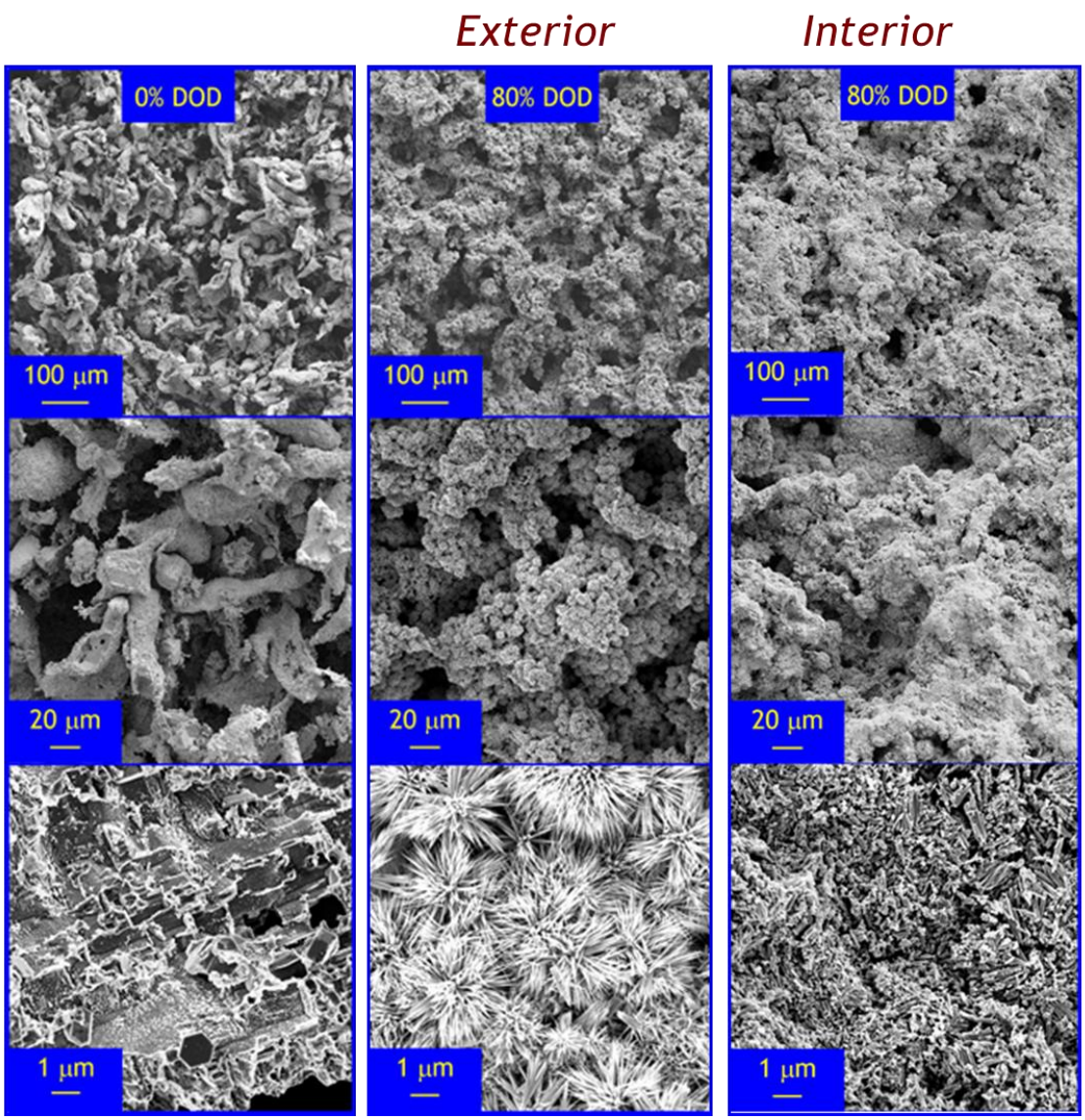

Figure S8. Scanning electron micrographs of the Zn sponge microstructure in its (**left**) pre–discharged state and after discharging to 80% DOD, revealing the progression of ZnO formation in the (**middle**) exterior/separator-facing boundary and (**right**) interior of the Zn sponge anode. (Alternate view of Figures 2 & 3)